 CMES, vol.71, no.1, pp.15-37, 2011

Numerical Simulations for Coupled Pair of Diffusion Equations by MLPG Method

S. Abbasbandy[1,2], V. Sladek[3], A. Shirzadi[1] and J. Sladek[3]

Abstract: This paper deals with the development of a new method for solution of initial-boundary value problems governed by a couple of nonlinear diffusion equations occurring in the theory of self-organization in non-equilibrium systems. The time dependence is treated by linear interpolation using the finite difference method and the semi-discrete partial differential equations are considered in a weak sense by using the local integral equation method with approximating 2-d spatial variations of the field variables by the Moving Least Squares. The evaluation techniques are discussed and the applicability of the presented method is demonstrated on two illustrative examples with exact solutions being used as benchmark solutions.

Keywords: MLPG, Moving least squares approximation, Numerical integration procedures, System of parabolic partial differential equations, Boundary conditions.

1 Introduction

According to the theory of self-organization in nonequilibrium systems [Nicolis and Prigogine (1977); Haken (1978); Ebeling (1976)] there are common principles of spontaneous creation of spatial and/or temporal structures in various disordered systems known from physics, chemistry, biology, sociology etc. Lot of such phenomena have been studied by [Lotka (1956); Volterra (1931); Turing (1952); Prigogine and Nicolis (1967); Prigogine and Lefever (1968); Zhabotinskiy (1964); Schlögl (1971a); Schlögl (1971b); Schlögl (1972); Haken (1975); Moore and Flaherty (1992)]. The Turing reaction-diffusion model [Turing (1952)] is the paradigm model for biological pattern formation. This model, a coupled system

[1] Department of Mathematics, Imam Khomeini International University, Ghazvin 34149, Iran
[2] *Corresponding author, Tel.: +98-912-1305326; fax: +98-281-3780040; E-mail address: abbasbandy@ikiu.ac.ir (S. Abbasbandy)
[3] Institute of Construction and Architecture, Slovak Academy of Sciences, 84503 Bratislava, Slovakia

of parabolic partial differential equations, has the counter-intuitive feature that diffusion can drive a spatially uniform stable state to unstable leading to spatially non-uniform steady states. Turing model has been applied in many areas of science, e.g., to whole range of patterning phenomena in biology [Kondo and Asai (1995); Meinhardt (2009); Miura, Shiota, Morriss-Kay, and Maini (2006)], ecology [Segal (1972)], chemistry [Castets, Dulos, Boissonade, and De Kepper (1990); Ouyang and Swinney (1991)]. It is well known that isomorphism of differential equations governing different phenomena yields structural isomorphism of such phenomena. From the mathematical point of view, the governing equations are rather complex coupled nonlinear partial differential equations. That stimulated mathematicians and engineers in enhanced study of the subject including the development of computational techniques for numerical solutions. The aim of this paper is to present a new numerical method based on the MLPG method [T. Zhu, J.-D. Zhang and S. N. Atluri (1998);Atluri,S. N.; Shen, S. (2002)] for solution of coupled pair of nonlinear diffusion equations in two spatial dimensions. In two last decades, mesh-free methods have become popular and well developed in various branches of science and engineering. Practically it is impossible to give a comprehensive review of the literature devoted to the development and applications of mesh-free methods. We concentrate on weak formulation on local subdomains. Such an approach enables development of truly mesh-free formulations in contrast to the weak formulations considered in the global sense, where the background mesh is still required [Atluri, Han, and Shen (2003); Atluri (2004)]. Several mesh-free approximations are usually used for modeling spatial variations of field variables [Atluri (2004); Liu (2003)]. The Radial Basis Functions (RBF) and the Moving Least Squares (MLS) belong to the most frequently used approximations, for some references see [Ling and Kansa (2004); Ling and Hon (2005); Libre, Emdadi, Kansa, Shekarchi, and Rahimian (2009); Abbasbandy and Shirzadi (2010); Abbasbandy and Shirzadi (2011); Ching and Batra (2001)]. In this paper, the time dependence is approximated by linear interpolation within each time step using the one-step-method [Smith (1978)]. Then, the original parabolic PDEs are converted into elliptic ones for the field variables at discrete time instants. Considering the local weak form of the developed elliptic PDEs with using the Heaviside-type of test functions, we employ the MLS approximation [Lancaster and Salkauskas (1981)] for spatial variations of the field variables at discrete time instants. Certain approximations are assumed for the evaluation of the domain integrals and the standard Gaussian quadrature is employed for the numerical evaluation of the boundary integrals occurring in the weak formulation. Finally, two numerical examples are considered in order to illustrate the applicability of the developed method to solution of the initial-boundary value problems for considered coupled parabolic PDEs. As compared with the similar method applied to simple diffusion equation [Sladek,

Sladek, and Atluri (2004); Sladek, Sladek, Tanaka, and Zhang (2005); Sladek, Sladek, Tan, and Atluri (2008)], in the first example, the governing equations are given by nonlinear pair of coupled diffusion equations. In the second example, the coupled pair of the diffusion equations is linear, but the exact solutions for the considered initial-boundary value problem exhibit both the rapid and smooth changes in various segments of the considered time interval. Then, it is demonstrated how the relaxed time spacing can be efficiently used for increasing the accuracy of the solution.

2 Two Governing equations, initial and boundary conditions

In this paper, we present an efficient numerical scheme for the following system of partial differential equations:

$$\begin{aligned} \frac{\partial u}{\partial t} &= \left(\frac{\partial^2 u}{\partial x^2}+\frac{\partial^2 u}{\partial y^2}\right)+k_1 u+r_1 f_1(u,v)+g_1(x,y,t), \\ \frac{\partial v}{\partial t} &= \left(\frac{\partial^2 v}{\partial x^2}+\frac{\partial^2 v}{\partial y^2}\right)+k_2 v+r_2 f_2(u,v)+g_2(x,y,t), \end{aligned} \tag{1}$$

in the two-dimensional region Ω, where k_1, r_1, k_2, and r_2 are suitably given constants. f_1 and f_2 are functions of the field variables u and v, g_1 and g_2 are assumed to be prescribed sources. The initial conditions are given as

$$\begin{aligned} u(x,y,0) &= f(x,y), \\ v(x,y,0) &= g(x,y), \end{aligned} \tag{2}$$

and Dirichlet boundary condition:

$$\begin{aligned} &u(x,y,t)=q_1(x,y,t), \quad (x,y) \in \partial\Omega \times t,\ t>0, \\ &v(x,y,t)=q_2(x,y,t). \end{aligned}$$

All the functions f_1, f_2, g_1, g_2, f, g, q_1, and q_2 are not specified from the point of view of the development of the computational method. Note that the present model is rather general and involves the well known models such as Turing model [Turing (1952)], prey-predator model and Lotka-Volterra model [Lotka (1956); Volterra (1931)] and many others.

3 MLS approximation for spatial variations of field variables

A meshless method uses a local interpolation or approximation to represent the trial function with the values of the unknown variable at some nodes. The moving least

squares (MLS) approximation is used on both meshless LBIE and MLPG methods which are used in this study and so is described in this section. Consider a sub-domain $\Omega_{\mathbf{x}}$, the neighborhood of a point $\mathbf{x}$ and denoted as the domain of definition of the MLS approximation for the trial function at $\mathbf{x}$, which is located in the problem domain Ω. To approximate the distribution of function u in $\Omega_{\mathbf{x}}$, over a number of randomly located nodes $\mathbf{x}_i, i = 1,2,...n$, the Moving Least Squares approximant $u^h(\mathbf{x})$ of u, $\forall \mathbf{x} \in \Omega_{\mathbf{x}}$, can be defined by

$$u^h(\mathbf{x}) = \mathbf{p}^T(\mathbf{x})\,\mathbf{a}(\mathbf{x}) \quad \forall \mathbf{x} \in \Omega_{\mathbf{x}}, \tag{3}$$

where $\mathbf{p}^T(\mathbf{x}) = [p_1(\mathbf{x}), p_2(\mathbf{x}), \ldots, p_m(\mathbf{x})]$ is a complete monomial basis of order m; and $a(\mathbf{x})$ is a vector containing coefficients $a_j(\mathbf{x}), j = 1,2,...m$ which are functions of the space coordinates $\mathbf{x}$. For example, for a 2-D problem, $\mathbf{p}^T(\mathbf{x}) = [1,x,y]$ and $\mathbf{p}^T(\mathbf{x}) = [1,x,y,x^2,xy,y^2]$, for linear basis ($m = 3$) and quadratic basis ($m = 6$), respectively.

The coefficient vector $\mathbf{a}(\mathbf{x})$ is determined by minimizing a weighted discrete L_2 norm, defined as

$$\begin{aligned} J(x) &= \sum_{i=1}^{n} w_i(\mathbf{x})[p^T(\mathbf{x}_i)\mathbf{a}(\mathbf{x}) - \hat{u}_i]^2 \\ &= [\mathbf{P}.\mathbf{a}(\mathbf{x}) - \hat{\mathbf{u}}]^T.W.[\mathbf{P}.\mathbf{a}(\mathbf{x}) - \hat{\mathbf{u}}], \end{aligned} \tag{4}$$

where $w_i(\mathbf{x})$ is the weight function associated with the node i, with $w_i(\mathbf{x}) > 0$ for all $\mathbf{x}$ in the support of $w_i(\mathbf{x})$,$\mathbf{x}_i$ denotes the value of $\mathbf{x}$ at node i, n is the number of nodes in $\Omega_{\mathbf{x}}$ for which the weight functions $w_i(\mathbf{x}) > 0$, the matrices $\mathbf{P}$ and $\mathbf{W}$ are defined as

$$\mathbf{P} = \begin{pmatrix} \mathbf{p}^T(\mathbf{x}_1) \\ \mathbf{p}^T(\mathbf{x}_2) \\ \ldots \\ \mathbf{p}^T(\mathbf{x}_n) \end{pmatrix}_{n \times m},$$

$$\mathbf{W} = \begin{pmatrix} w_1(\mathbf{x}) & \ldots & 0 \\ \ldots & \ldots & \ldots \\ 0 & \ldots & w_n(\mathbf{x}) \end{pmatrix},$$

and $\hat{\mathbf{u}}^T = [\hat{u}_1, \hat{u}_2, ..., \hat{u}_n]$. Here it should be noted that $\hat{u}_i,\ i = 1,2,...,n$ in (4) are the fictitious nodal values, and not the nodal values of the unknown trial function $u^h(\mathbf{x})$ in general. The stationarity of J in (4) with respect to $\mathbf{a}(\mathbf{x})$ leads to the following linear relation between $\mathbf{a}(\mathbf{x})$ and $\hat{\mathbf{u}}$

$$\mathbf{A}(\mathbf{x})\mathbf{a}(\mathbf{x}) = \mathbf{B}(\mathbf{x})\hat{\mathbf{u}}, \tag{5}$$

where the matrices $\mathbf{A}(\mathbf{x})$ and $\mathbf{B}(\mathbf{x})$ are defined by

$$\mathbf{A}(\mathbf{x}) = \mathbf{P}^T\mathbf{W}\mathbf{P} = \mathbf{B}(\mathbf{x})\mathbf{P} = \sum_{i=1}^{n} w_i(\mathbf{x})\mathbf{p}(\mathbf{x}_i)\mathbf{p}^T(\mathbf{x}_i), \tag{6}$$

$$\mathbf{B}(\mathbf{x}) = \mathbf{P}^T\mathbf{W} = [w_1(\mathbf{x})\mathbf{p}(\mathbf{x}_1), w_2(\mathbf{x})\mathbf{p}(\mathbf{x}_2), ..., w_n(\mathbf{x})\mathbf{p}(\mathbf{x}_n)]. \tag{7}$$

The MLS approximation is well defined only when the matrix $\mathbf{A}$ in (5) is non-singular. It can be seen that this is the case if and only if the rank of $\mathbf{P}$ equals m. A necessary condition for a well-defined MLS approximation is that at least m weight functions are non-zero (i.e. $n > m$) for each sample point $\mathbf{x} \in \Omega$ and that the nodes in $\Omega_{\mathbf{x}}$ will not be arranged in a special pattern such as on a straight line. Here a sample point may be a nodal point under consideration or a quadrature point.

Solving for $\mathbf{a}(\mathbf{x})$ from (5) and substituting it into (3) gives a relation which may be written as the form of an interpolation function similar to that used in FEM, as

$$u^h(\mathbf{x}) = \Phi^T(\mathbf{x}).\hat{\mathbf{u}} = \sum_{i=1}^{n} \phi_i(\mathbf{x})\hat{u}_i; \;\; u^h(\mathbf{x}_i) \equiv u_i; \quad \mathbf{x} \in \Omega_{\mathbf{x}}, \tag{8}$$

and essentially $u_i \neq \hat{u}_i$, where

$$\Phi^T(\mathbf{x}) = \mathbf{p}^T(\mathbf{x})\mathbf{A}^{-1}(\mathbf{x})\mathbf{B}(\mathbf{x}), \tag{9}$$

or

$$\phi_i(\mathbf{x}) = \sum_{j=1}^{m} p_j(\mathbf{x})[\mathbf{A}^{-1}(\mathbf{x})\mathbf{B}(\mathbf{x})]_{ji}.$$

$\phi_i(\mathbf{x})$ is usually called the shape function of the MLS approximation corresponding to nodal point y_i. From (7) and (9), it may be seen that $\phi_i(\mathbf{x}) = 0$ when $w_i(\mathbf{x}) = 0$. In practical applications, $w_i(\mathbf{x})$ is generally chosen such that it is non-zero over the support of nodal points y_i. The support of the nodal point y_i is usually taken to be a circle of radius r_i, centered at y_i. The fact that $\phi_i(\mathbf{x}) = 0$, for $\mathbf{x}$ not in the support of nodal point y_i preserves the local character of the Moving Least Squares approximation.

Let $C^q(\Omega)$ be the space of qth continuously differentiable functions on Ω. If $w_i(\mathbf{x}) \in C^q(\Omega)$ and $p_j(\mathbf{x}) \in C^s(\Omega)$, $\;i = 1,2,...,n, \;\; j = 1,2,...,m$, then $\phi_i(\mathbf{x}) \in C^r(\Omega)$ with $r = \min(q,s)$.

The partial derivatives of $\phi_i(\mathbf{x})$ are obtained as

$$\phi_{i,k} = \sum_{j=1}^{m} [p_{j,k}(\mathbf{A}^{-1}\mathbf{B})_{ji} + p_j(\mathbf{A}^{-1}\mathbf{B}_{,k} + \mathbf{A}^{-1}_{,k}\mathbf{B})_{ji}], \tag{10}$$

in which $\mathbf{A}^{-1}_{,k} = (\mathbf{A}^{-1})_{,k}$ represents the derivative of the inverse of A with respect to x_k, which is given by $\mathbf{A}^{-1}_{,k} = -\mathbf{A}^{-1}\mathbf{A}_{,k}\mathbf{A}^{-1}$, where$(\ )_{,i}$ denotes $\partial(\ )/\partial x_i$.
In this paper the Gaussian weight function is used as

$$w_i(\mathbf{x}) = \begin{cases} \frac{exp[-(\frac{d_i}{c_i})^2]-exp[-(\frac{r_i}{c_i})^2]}{1-exp[-(\frac{r_i}{c_i}^2)]}, & 0 \le d_i \le r_i, \\ 0, & d_i \ge r_i, \end{cases}$$

where $d_i = \| x - x_i \|$, c_i is a constant controlling the shape of the weight function w_i and r_i is the size of the support domain.

The size of support, r_i, of the weight function w_i associated with node i should be chosen such that r_i should be large enough to have sufficient number of nodes covered in the domain of definition of every sample point $(n \ge m)$ to ensure the regularity of $\mathbf{A}$. On the other hand, r_i should also be small enough to maintain the local character of the MLS approximation.

4 The numerical solution procedure

4.1 The time discretization

The finite-difference approximation of the time derivatives in the θ method is given as follows

$$\theta \dot{u}^{k+1} + (1-\theta)\dot{u}^k = \frac{u^{k+1}-u^k}{\Delta t}, \qquad 0 \le \theta \le 1. \tag{11}$$

Considering Eq. (1) at the time instants $k\Delta t$ and $(k+1)\Delta t$, one obtains, respectively

$$\begin{aligned} \theta \dot{u}^{k+1} &= \theta\nabla^2 u^{k+1} + \theta k_1 u^{k+1} + \theta r_1 f_1(u^{k+1}, v^{k+1}) + \theta g_1(x, y, (k+1)\Delta t), \\ (1-\theta)\dot{u}^k &= (1-\theta)\nabla^2 u^k + (1-\theta)k_1 u^k + (1-\theta)r_1 f_1(u^k, v^k) + (1-\theta)g_1(x, y, k\Delta t). \end{aligned}$$

Hence and from (11), we have

$$\begin{aligned} &\frac{u^{k+1}-u^k}{\Delta t} = \nabla^2 u^k + \theta\left(\nabla^2 u^{k+1} - \nabla^2 u^k\right) + k_1\left[u^k + \theta\left(u^{k+1}-u^k\right)\right] \\ &+ r_1\left[f_1^k + \theta\left(f_1^{k+1} - f_1^k\right)\right] + g_1^k + \theta\left(g_1^{k+1} - g_1^k\right). \end{aligned} \tag{12}$$

In the case of Crank-Nicholson scheme ($\theta = \frac{1}{2}$) Eq. (12) becomes:

$$\frac{u^{k+1}-u^k}{\Delta t} = \frac{1}{2}\left(\nabla^2 + k_1\right)\left(u^{k+1}+u^k\right) + \frac{r_1}{2}\left(f_1^{k+1}+f_1^k\right) + \frac{1}{2}\left(g_1^{k+1}+g_1^k\right)$$

or

$$\left[1-\frac{\Delta t}{2}\left(k_1+\nabla^2\right)\right]u^{k+1}-\frac{r_1\Delta t}{2}f_1^{k+1} \tag{13}$$
$$=\left[1+\frac{\Delta t}{2}\left(k_1+\nabla^2\right)\right]u^{k}+\frac{r_1\Delta t}{2}f_1^{k}+\frac{\Delta t}{2}\left(g_1^{k+1}+g_1^{k}\right).$$

Similarly, we have

$$\left[1-\frac{\Delta t}{2}\left(k_2+\nabla^2\right)\right]v^{k+1}-\frac{r_2\Delta t}{2}f_2^{k+1}= \tag{14}$$
$$\left[1+\frac{\Delta t}{2}\left(k_2+\nabla^2\right)\right]v^{k}+\frac{r_2\Delta t}{2}f_2^{k}+\frac{\Delta t}{2}\left(g_2^{k+1}+g_2^{k}\right).$$

Thus, the parabolic PDEs are replaced by the semi-discrete PDEs of the elliptic type for the field variables u^{k+1} and v^{k+1}, assuming the fields u^k and v^k being known from the computation in the previous time step.

The further steps in solution of these equations depends on the character of functions f_1 and f_2. In general, one should solve them iteratively in each time step with replacing f_1^{k+1} and f_2^{k+1} by f_1^k and f_2^k, respectively, at the zeroth iteration. If these functions are sufficiently smooth, one can solve linearized equations

$$\left[1-\frac{\Delta t}{2}\left(r_1f_{1,u}^{k}+k_1+\nabla^2\right)\right]u^{k+1}-\frac{r_1\Delta t}{2}f_{1,v}^{k}v^{k+1}=$$
$$\left[1+\frac{\Delta t}{2}\left(-r_1f_{1,u}^{k}+k_1+\nabla^2\right)\right]u^{k}-\frac{r_1\Delta t}{2}f_{1,v}^{k}v^{k}+r_1\Delta t f_1^k+\frac{\Delta t}{2}\left(g_1^{k+1}+g_1^{k}\right),$$
$$\left[1-\frac{\Delta t}{2}\left(r_2f_{2,v}^{k}+k_2+\nabla^2\right)\right]v^{k+1}-\frac{r_2\Delta t}{2}f_{2,u}^{k}u^{k+1}=$$
$$\left[1+\frac{\Delta t}{2}\left(-r_2f_{2,v}^{k}+k_2+\nabla^2\right)\right]v^{k}-\frac{r_2\Delta t}{2}f_{2,u}^{k}u^{k}+r_2\Delta t f_2^k+\frac{\Delta t}{2}\left(g_2^{k+1}+g_2^{k}\right),$$

instead of using the iterative procedure.

4.2 The local weak formulation of the time-stepping semi-discrete PDEs

We construct the weak form over local nodal based sub-domains such as Ω_s, which is a small region taken for each node in the global domain Ω. The local sub-domains could be of any geometric shape and size. In this paper they are taken to be of circular shape. The local weak form of the equations (13,14) for $\mathbf{x}^i=(x^i,y^i)\in\Omega_{s^i}$

can be written as

$$\int_{\Omega_{si}} \left[\left[1-\frac{\Delta t}{2}\left(k_1+\nabla^2\right)\right]u^{k+1}-\frac{r_1\Delta t}{2}f_1^{k+1}\right]u^* d\mathbf{x} \tag{15}$$
$$=\int_{\Omega_{si}} \left[\left[1+\frac{\Delta t}{2}\left(k_1+\nabla^2\right)\right]u^{k}+\frac{r_1\Delta t}{2}f_1^{k}+\frac{\Delta t}{2}\left(g_1^{k+1}+g_1^{k}\right)\right]u^* d\mathbf{x},$$

$$\int_{\Omega_{si}} \left[\left[1-\frac{\Delta t}{2}\left(k_2+\nabla^2\right)\right]v^{k+1}-\frac{r_2\Delta t}{2}f_2^{k+1}\right]u^* d\mathbf{x} \tag{16}$$
$$=\int_{\Omega_{si}} \left[\left[1+\frac{\Delta t}{2}\left(k_2+\nabla^2\right)\right]v^{k}+\frac{r_2\Delta t}{2}f_2^{k}+\frac{\Delta t}{2}\left(g_2^{k+1}+g_2^{k}\right)\right]u^* d\mathbf{x}$$

where u^* is a test function, u and v are trial functions, and instead of the entire domain Ω we have considered a sub-domain Ω_{si} located entirely inside Ω which is a circle of radius r_0 and centered at node $\mathbf{x}^i$. If the Heaviside step function

$$u^*(\mathbf{x})=\begin{cases} 1, & \mathbf{x}\in\Omega_s, \\ 0, & \mathbf{x}\notin\Omega_s, \end{cases}$$

is chosen as the test function in each sub-domain , then $\nabla u^*=0$ and from the relation

$$\int_{\Omega_{si}} u^*\nabla^2 u d\mathbf{x}=\int_{\Omega_{si}} \nabla u\nabla u^* d\mathbf{x}+\int_{\partial\Omega_{si}} u^*\frac{\partial u}{\partial n}d\mathbf{s}$$

we have

$$\int_{\Omega_{si}} \nabla^2 u d\mathbf{x}=\int_{\partial\Omega_{si}} \frac{\partial u}{\partial n}d\mathbf{s}$$

and so the local weak forms (15) and (16) are transformed into the following simple equations

$$\left(1-\frac{k_1\Delta t)}{2}\right)\int_{\Omega_{si}} u^{k+1}d\mathbf{x}-\frac{\Delta t}{2}\int_{\partial\Omega_{si}}\frac{\partial u^{k+1}}{\partial n}d\mathbf{s}$$
$$-\frac{r_1\Delta t}{2}\int_{\Omega_{si}} f_1^{k+1}d\mathbf{x}=\left(1+\frac{k_1\Delta t)}{2}\right)\int_{\Omega_{si}} u^{k}d\mathbf{x}+\frac{\Delta t}{2}\int_{\partial\Omega_{si}}\frac{\partial u^{k}}{\partial n}d\mathbf{s} \tag{17}$$
$$+\frac{r_1\Delta t}{2}\int_{\Omega_{si}} f_1^{k}d\mathbf{x}+\frac{\Delta t}{2}\int_{\Omega_{si}}\left(g_1^{k+1}+g_1^{k}\right)d\mathbf{x},$$

$$\begin{aligned}
&\Big(1-\frac{k_2\Delta t}{2}\Big)\int_{\Omega_{s^i}} v^{k+1}d\mathbf{x}-\frac{\Delta t}{2}\int_{\partial\Omega_{s^i}}\frac{\partial v^{k+1}}{\partial n}d\mathbf{s}\\
&-\frac{r_2\Delta t}{2}\int_{\Omega_{s^i}} f_2^{k+1}d\mathbf{x}=\Big(1+\frac{k_2\Delta t)}{2}\Big)\int_{\Omega_{s^i}} v^{k}d\mathbf{x}+\frac{\Delta t}{2}\int_{\partial\Omega_{s^i}}\frac{\partial v^{k}}{\partial n}d\mathbf{s}\\
&+\frac{r_2\Delta t}{2}\int_{\Omega_{s^i}} f_2^{k}d\mathbf{x}+\frac{\Delta t}{2}\int_{\Omega_{s^i}}\Big(g_2^{k+1}+g_2^{k}\Big)d\mathbf{x}.
\end{aligned}\tag{18}$$

4.3 Discretization of the local weak forms and imposing boundary condition

Consider N nodal points on the boundary and domain of the problem of which M of them are located on the domain and L of them on the boundary. Assuming that $\hat{u}_i^k$, for $i=1,2,...,N$ is known, our aim is to compute $\hat{u}_i^{k+1}$, for $i=1,2,...,N$ in the time stepping technique. So we have N unknowns and to compute these unknowns we need N equations. For nodes which are located on the boundaries, we have

$$\begin{aligned}
&\sum_{j=1}^{N}\phi_j(\mathbf{x}^i)\hat{u}_j^{k+1}=q_1(\mathbf{x}^i,(k+1)\Delta t),\\
&\sum_{j=1}^{N}\phi_j(\mathbf{x}^i)\hat{v}_j^{k+1}=q_2(\mathbf{x}^i,(k+1)\Delta t).
\end{aligned}\tag{19}$$

For nodes which are located in the interior of the domain, i.e., for $\mathbf{x}^i\in$ interior Ω, from (17) and (18) and using the MLS approximation (8), we have the following equations

$$\begin{aligned}
&\Big(1-\frac{k_1\Delta t)}{2}\Big)\sum_{j=1}^{N}\Big(\int_{\Omega_{s^i}}\phi_j d\mathbf{x}\Big)\hat{u}_j^{k+1}\\
&-\frac{\Delta t}{2}\sum_{j=1}^{N}\Big(\int_{\partial\Omega_{s^i}}\frac{\partial\phi_j}{\partial n}d\mathbf{s}\Big)\hat{u}_j^{k+1}-\frac{r_1\Delta t}{2}\int_{\Omega_{s^i}}\tilde{f}_1^{k+1}d\mathbf{x}=\\
&\Big(1+\frac{k_1\Delta t)}{2}\Big)\sum_{j=1}^{N}\Big(\int_{\Omega_{s^i}}\phi_j d\mathbf{x}\Big)\hat{u}_j^{k}+\frac{\Delta t}{2}\sum_{j=1}^{N}\Big(\int_{\partial\Omega_{s^i}}\frac{\partial\phi_j}{\partial n}d\mathbf{s}\Big)\hat{u}_j^{k}\\
&+\frac{r_1\Delta t}{2}\int_{\Omega_{s^i}}\tilde{f}_1^{k}d\mathbf{x}+\frac{\Delta t}{2}\int_{\Omega_{s^i}}\Big(g_1^{k+1}+g_1^{k}\Big)d\mathbf{x},
\end{aligned}\tag{20}$$

$$\Big(1-\frac{k_2\Delta t)}{2}\Big)\sum_{j=1}^{N}\Big(\int_{\Omega_{si}}\phi_j d\mathbf{x}\Big)\hat{v}_j^{k+1}-\frac{\Delta t}{2}\sum_{j=1}^{N}\Big(\int_{\partial\Omega_{si}}\frac{\partial\phi_j}{\partial n}d\mathbf{s}\Big)\hat{v}_j^{k+1} \tag{21}$$

$$-\frac{r_2\Delta t}{2}\int_{\Omega_{si}}\tilde{f}_2^{k+1}d\mathbf{x}=\Big(1+\frac{k_2\Delta t)}{2}\Big)\sum_{j=1}^{N}\Big(\int_{\Omega_{si}}\phi_j d\mathbf{x}\Big)\hat{v}_j^{k}+\frac{\Delta t}{2}\sum_{j=1}^{N}\Big(\int_{\partial\Omega_{si}}\frac{\partial\phi_j}{\partial n}d\mathbf{s}\Big)\hat{v}_j^{k}$$

$$+\frac{r_2\Delta t}{2}\int_{\Omega_{si}}\tilde{f}_2^{k}d\mathbf{x}+\frac{\Delta t}{2}\int_{\Omega_{si}}\Big(g_2^{k+1}+g_2^{k}\Big)d\mathbf{x},$$

where

$$\tilde{f}_i^k=f_i(\tilde{u}^k(\mathbf{x}),\tilde{v}^k(\mathbf{x})),\qquad i=1,2,$$
$$\tilde{u}^k(\mathbf{x})=\sum_{j=1}^{N}\phi_j(\mathbf{x})\hat{u}_j^k,\qquad \tilde{v}^k(\mathbf{x})=\sum_{j=1}^{N}\phi_j(\mathbf{x})\hat{v}_j^k.$$

Note that the set of algebraic equations (19),(20) and (21) represent the discretized version of the local weak form of the original pair of coupled PDEs (1) with assuming the Crank-Nicholson scheme for the linear time interpolation within time steps and the standard MLS approximation for the spatial variations of the field variables.

4.4 Employed evaluation techniques and simplification approximations

In all examples, for the MLS approximation the quadratic basis ($m=6$) and the Gaussian weight function are utilized. The eight points Gauss-Legendre quadrature rule is used for the regular local boundary integrals as follow

$$\int_{\partial\Omega_{si}}\phi_j(\mathbf{x})d\mathbf{s}$$
$$=\int_0^{2\pi}\phi_j(x^i+r_0cos(\theta),y^i+r_0sin(\theta))r_0d\theta$$
$$=\pi r_0\int_{-1}^{1}\phi_j(x^i+r_0cos(\pi\theta+\pi),y^i+r_0sin(\pi\theta+\pi))d\theta$$
$$=\pi r_0\sum_{p=1}^{8}w_p\phi_j(x^i+r_0cos(\pi\theta_p+\pi),y^i+r_0sin(\pi\theta_p+\pi)),$$

where w_p and θ_p are the Gauss quadrature integration rule weights and points on [-1, 1]. The domain integrals appearing in the MLPG formulation are approximated

and computed as follows:

$$\int_{\Omega_{s^i}} \phi_j(\mathbf{x}) d\mathbf{x} \approx \phi_j(\mathbf{x}^i) \int_{\Omega_{s^i}} 1 d\mathbf{x} = \pi \phi_j(\mathbf{x}^i) r_0^2,$$

$$\int_{\Omega_{s^i}} \tilde{f}_1^k d\mathbf{x} \approx f_1(\tilde{u}^k(\mathbf{x}^i), \tilde{v}^k(\mathbf{x}^i)) \int_{\Omega_{s^i}} 1 d\mathbf{x} = \pi f_1(\tilde{u}^k(\mathbf{x}^i), \tilde{v}^k(\mathbf{x}^i)) r_0^2,$$

similarly, for $\tilde{f}_2^k$ we have $\int_{\Omega_{s^i}} \tilde{f}_2^k d\mathbf{x} \approx \pi f_2(\tilde{u}^k(\mathbf{x}^i), \tilde{v}^k(\mathbf{x}^i)) r_0^2$.

5 Test problems

The domain and boundary integrals are evaluated as demonstrated in the previous section. We recall that r_0 is the radius of each local sub-domains and r_i is the radius of the support of the weight function corresponding to node i. For the MLS approximations, the quadratic basis is used in this paper. The gaussian weight function is used for the MLS approximation and $c_i \approx 0.6h$, where h is the minimum distance between two consecutive nodes in each direction. In general, there is no restriction on the size of sub-domains in the local weak formulation. Nevertheless, because of the computational techniques described in the previous section, r_0 should be small enough. A very small r_0 also causes much cancellation error. So it is chosen as $0.001 \leq r_0 \leq 0.01$ in this paper, where the analyzed domain is $\Omega = [0,1] \times [0,1]$. For the moving least square moment matrix to be invertible, the support of weight functions, r_i, should be large enough to have sufficient number of nodes covered in the domain of definition of every sample point. On the other hand, it should be small enough to preserve the local character of the MLS approximation. In this paper it is chosen as $r_i \approx 3k$, where k is the maximum distance between two consecutive nodes. It should be noted that these parameters may depend on the problem under consideration, and the computational techniques used.
The infinity norm of error of u is represented by $\| e_u \|_\infty$ and that of v by $\| e_v \|_\infty$, where

$$\| e_u \|_\infty = max\{ | u_i - \hat{u}_i | , \qquad i = 1,2,...,N\},$$

u_i and $\hat{u}_i$ are the exact and approximate value of u at point $\mathbf{x}_i$, respectively, and N is the number of nodes.

Example 1. For the first test problem consider the following system of nonlinear

diffusive PDEs in the region $\Omega = [0,1] \times [0,1]$

$$\begin{aligned}
\frac{\partial u}{\partial t} &= \left(\frac{\partial^2 u}{\partial x^2} + \frac{\partial^2 u}{\partial y^2}\right) + u - u^2 + uv + g_1(x,y,t), \\
\frac{\partial v}{\partial t} &= \left(\frac{\partial^2 v}{\partial x^2} + \frac{\partial^2 v}{\partial y^2}\right) + 2v - v^2 + u^2 v + g_2(x,y,t),
\end{aligned}$$

where

$$\begin{aligned}
g_1(x,y,t) &= t^4(x-1)^2x^2(y-1)^2y^2 - t^2(x-1)x(y-1)y\left(-t+x^2+y^2\right) \\
&\quad -t^2(x-1)x(y-1)y - 2t^2(x-1)x - 2t^2(y-1)y + 2t(x-1)x(y-1)y, \\
g_2(x,y,t) &= t^4\left(-(x-1)^2\right)x^2(y-1)^2y^2\left(-t+x^2+y^2\right) \\
&\quad + \left(-t+x^2+y^2\right)^2 - 2\left(-t+x^2+y^2\right) - 5.
\end{aligned}$$

The initial and boundary conditions are chosen in such a way that the exact solution is:

$$\begin{aligned}
u(x,y,t) &= t^2(x-1)x(y-1)y, \\
v(x,y,t) &= -t+x^2+y^2,
\end{aligned}$$

see Fig. 1 for initial profile of v and u is initially zero. Since the functions f_1 and f_2 are nonlinear in this example, the algebraic equations (20) and (21) has been solved iteratively in each time step with replacing f_1^{k+1} and f_2^{k+1} by f_1^k and f_2^k, respectively, at the zeroth iteration. The results presented here are obtained with only one iteration.

The obtained results at $t = 2$, with $N = 111$ nodal points and various Δt are presented in Tab. 1. The results reveal that the accuracy of numerical solution increases as the size of time step becomes smaller. The obtained errors for different N and t are presented in Tab. 2 and Tab. 3, respectively. The graph of obtained solution for u and v are plotted in Fig. 2, Fig. 3, Fig. 4 and Fig. 5, respectively, for $N = 441$.

In order to show the convergence of our proposed iterative procedure, we present Tab. 4. In this table, corresponding to each iteration we have two rows for which the first row represents $\| e_u \|_\infty$ and the second row represents $\| e_v \|_\infty$. ITR refers to the number of iterations. The improvement of the accuracy during the iteration procedure is more clear for bigger Δt, e.g. $\Delta t = 0.1$ and 0.05 (the columns 1 and 2) and it is more significant for v (the second row in each iteration step).

For smaller time steps the accuracy is not further improved after the first or second iteration step owing to cancellation errors. The infinity norm of errors of numerical solutions obtained for u and v versus time variable t are presented in Fig. 5. In

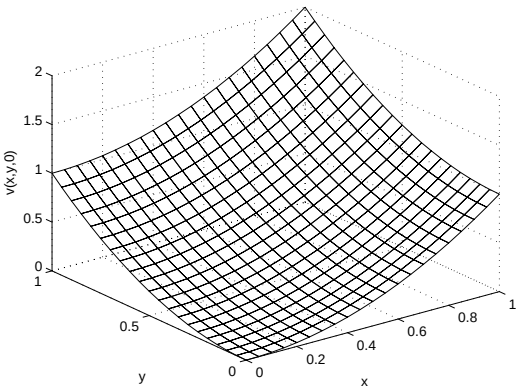

Figure 1: Initial profile of v

Table 1: Error with different Δt

Δt	$\| e_u \|_\infty$	$\| e_v \|_\infty$
0.1	1.212214×10^{-2}	9.411551×10^{-3}
0.05	6.351893×10^{-3}	4.700534×10^{-3}
0.01	1.756992×10^{-3}	9.233328×10^{-4}
0.005	1.183955×10^{-3}	4.506939×10^{-4}
0.001	7.257365×10^{-4}	7.250613×10^{-5}
0.0005	6.684724×10^{-4}	2.522788×10^{-5}

Table 2: Errors at $t = 2$, $\Delta t = 0.005$ for different number of nodal points

N	$\| e_u \|_\infty$	$\| e_v \|_\infty$
81	1.527797×10^{-3}	4.356309×10^{-4}
121	1.183955×10^{-3}	4.506939×10^{-4}
289	8.115125×10^{-4}	4.655717×10^{-4}
441	7.2568178×10^{-4}	4.711232×10^{-4}

Table 3: Errors at different time instants with $N = 441$ nodal points and $\Delta t = 0.005$

t	$\| e_u \|_\infty$	$\| e_v \|_\infty$
0.2	6.451428×10^{-5}	3.816598×10^{-4}
0.4	1.315446×10^{-4}	4.009743×10^{-4}
0.6	2.005670×10^{-4}	4.111255×10^{-4}
0.8	2.714080×10^{-4}	4.213505×10^{-4}
1	3.439055×10^{-4}	4.317110×10^{-4}
1.5	5.313506×10^{-4}	4.560768×10^{-4}
2	7.256817×10^{-4}	4.711232×10^{-4}

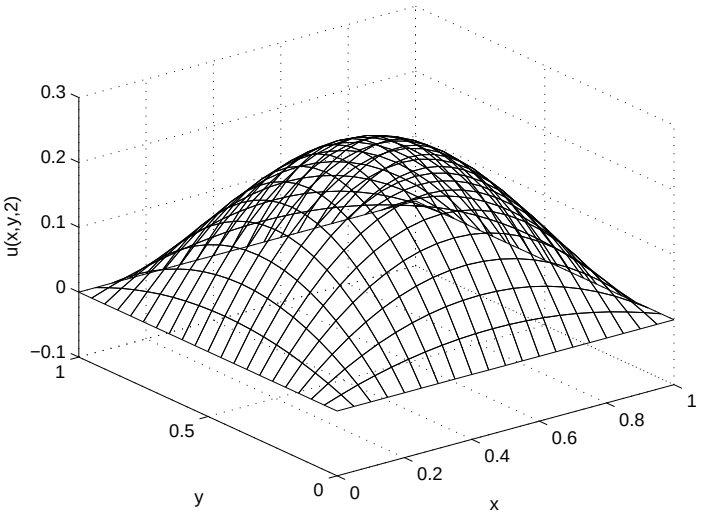

Figure 2: Numerical solution obtained for u at $t = 2$, using $N = 441$ nodal points and $\Delta t = 0.001$

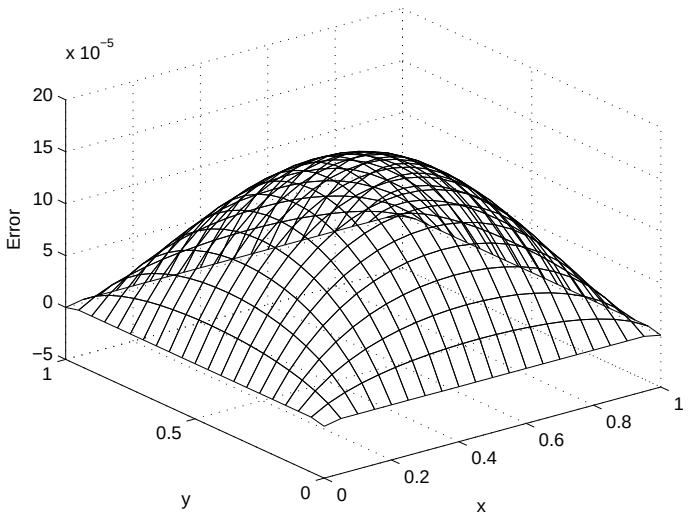

Figure 3: Error distribution for u at $t = 2$ in Example 1

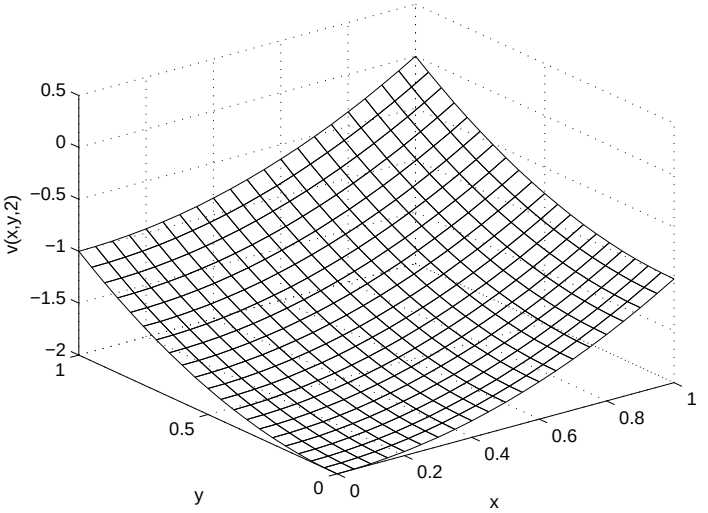

Figure 4: Numerical solution obtained for v at $t = 2$, using $N = 441$ nodal points and $\Delta t = 0.001$

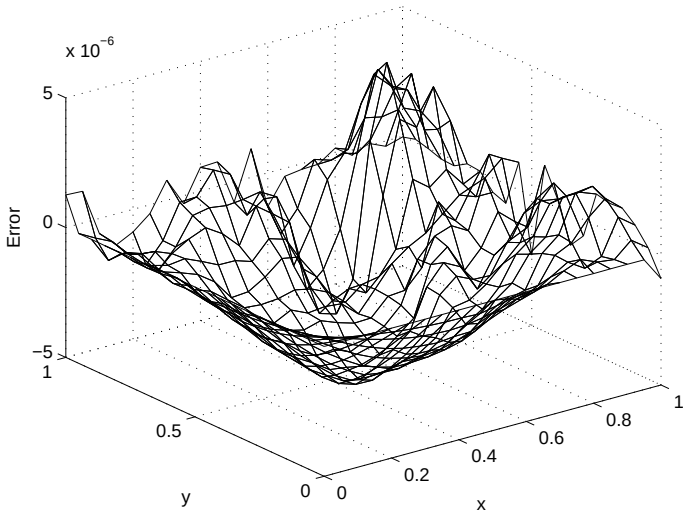

Figure 5: Error distribution for v at $t = 2$ in Example 1

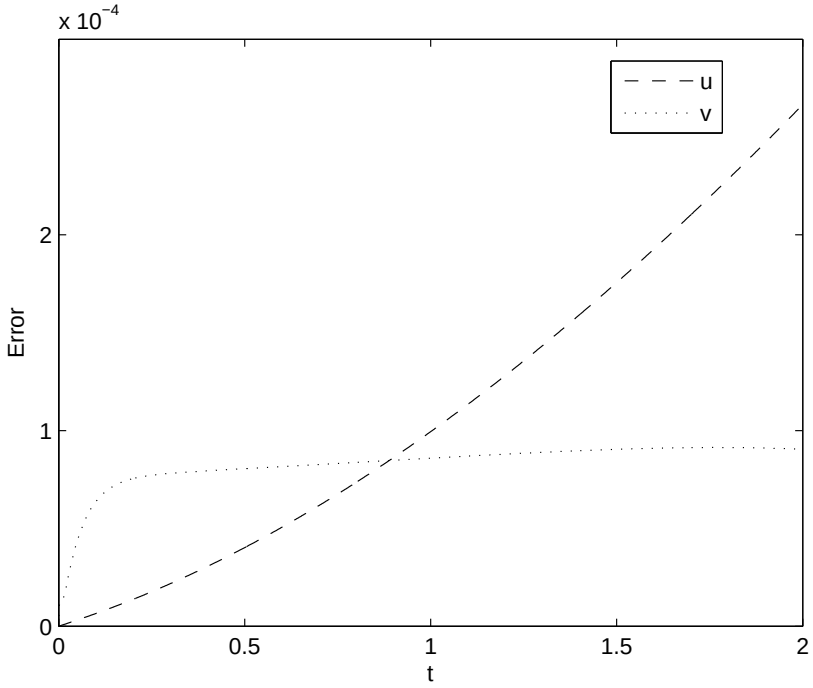

Figure 6: Errors versus time t with N=441 nodal points and $\Delta t = 0.001$

Table 4: Errors at $t = 0.5$ with $N = 441$ nodal points, various iterations and Δt

$\Delta t \rightarrow$	0.1	0.05	0.01	0.005
ITR=0	2.507646×10^{-5}	1.041082×10^{-5}	7.795428×10^{-6}	8.005067×10^{-6}
	0.001999	0.001019	2.030702×10^{-4}	1.006921×10^{-4}
ITR=1	9.241597×10^{-6}	8.914953×10^{-6}	8.787914×10^{-6}	8.783149×10^{-6}
	4.957661×10^{-5}	2.009308×10^{-5}	1.225472×10^{-5}	1.205132×10^{-5}
ITR=2	8.774170×10^{-6}	8.780075×10^{-6}	8.781492×10^{-6}	8.781507×10^{-6}
	2.354149×10^{-5}	8.235863×10^{-6}	1.195439×10^{-5}	1.195798×10^{-5}
ITR=3	8.780696×10^{-6}	8.781343×10^{-6}	8.781503×10^{-6}	8.781509×10^{-6}
	2.373307×10^{-5}	8.370234×10^{-6}	1.195602×10^{-5}	1.195829×10^{-5}
ITR=4	8.780595×10^{-6}	8.781327×10^{-6}	8.781503×10^{-6}	8.781509×10^{-6}
	2.372902×10^{-5}	8.3684370×10^{-6}	1.195601×10^{-5}	1.195829×10^{-5}

Fig. 5, we can see increasing inaccuracy of u with increasing time. Moreover, in the case of v we can see different behavior. A reason for this is that the dependence of u on the time variable t is quadratic, whereas the dependence of v on the time variable is linear. The latter is much better approximated by the employed finite-difference approximation (11).

Example 2. For the second test problem consider the system of linear parabolic PDEs

$$\begin{aligned}\frac{\partial u}{\partial t} &= \left(\frac{\partial^2 u}{\partial x^2}+\frac{\partial^2 u}{\partial y^2}\right)+v,\\ \frac{\partial v}{\partial t} &= \left(\frac{\partial^2 v}{\partial x^2}+\frac{\partial^2 v}{\partial y^2}\right)+16u,\end{aligned}$$

in the two-dimensional region $\Omega = [0,1]\times[0,1]$. The initial and boundary conditions are chosen in such a way that the exact solution is:

$$\begin{aligned}u(x,y,t) &= exp(x+y-2t),\\ v(x,y,t) &= -4exp(x+y-2t).\end{aligned}$$

All calculations for this example are performed with N=441 nodal points. The max norm of obtained numerical solutions and the corresponding max error are presented in Fig. 7 and Fig. 8, respectively.

The max norm of u at time instant t_k, or $\| u^k \|_\infty$, is defined as:

$$\| u^k \|_\infty = max\{| u_i^k |, \qquad i = 1,2,...,N\},$$

where $u_i^k = u(\mathbf{x}_i, k\Delta t)$, and N is the number of nodes.

It can be seen from Fig. 8 that the errors have an increase near initial time $t = 0$, and then decrease. This is more significant for the function v. This can be explained by very rapid temporal changes of the solutions near the initial time and relatively smooth variation at later time instants. For this kind of problems, we can obtain more accurate solutions by using variable length of the time steps; so that the time step be very small at time $t = 0$ and it can be larger when t increases. Choosing a very small and fixed time step is much time consuming and not necessary. So, we define a measure between the numerical solutions $U(x,.)$ of two consecutive time steps by

$$\Delta U_{t_k} = \| u^k(\mathbf{x}) - u^{k-1}(\mathbf{x}) \|_\infty, \qquad for\ \ k = 1,2,...,K. \tag{22}$$

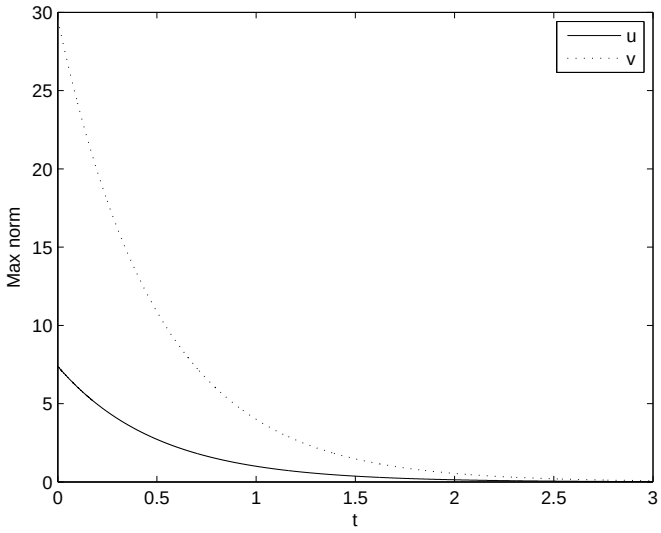

Figure 7: Max norm of numerical solutions obtained with N=441 nodal points and $\Delta t = 0.0005$ for Example 2

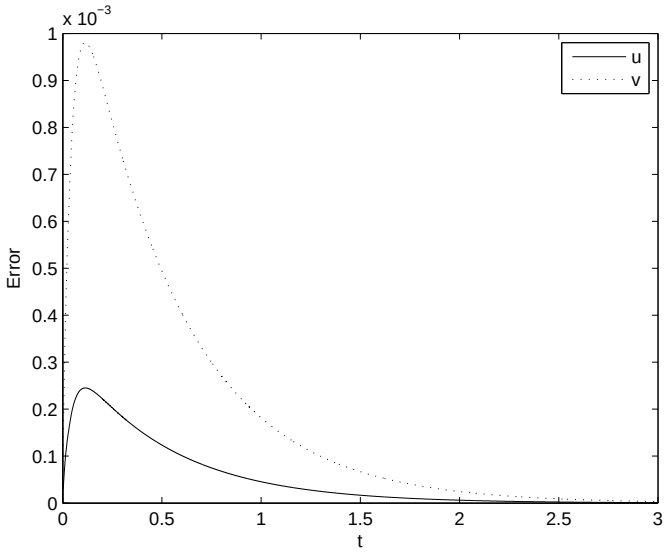

Figure 8: Max error of numerical solutions obtained with fixed $\Delta t = 0.0005$ for Example 2

For some user-defined relaxation parameters τ, if $\Delta U_{t_k} < \tau$, the time spacing is relaxed:

$$\Delta t \leftarrow 2\Delta t$$

up to some prefixed value Δt_{max}. See Fig. 9 and Fig. 10 for maximum error obtained for different values of Δt and τ. See also [Brunner, Ling, and Yamamoto (2010)] for more useful information in this regard.

6 Conclusions

The weak formulation based on meshless implementation of local integral equations developed for diffusion equation has been successfully extended to a pair of coupled nonlinear diffusion equations. The time variations are treated by using the finite difference method with relaxed time spacing and the nonlinearities by iterative technique within each time step. The developed method supplemented with several computational techniques has been verified on test examples with using the exact solution as benchmark solutions.

Acknowledgement: The authors (V. Sladek and J. Sladek) gratefully acknowledge the support by the Slovak Science and Technology Assistance Agency registered under number APVV-0032-10 and the Slovak Grant Agency VEGA-2/0039/09.

References

Abbasbandy, S.; Shirzadi, A. (2010): A meshless method for two-dimensional diffusion equation with an integral condition. *Eng. Anal. Bound. Elem.*, vol. 34, pp. 1031–1037.

Abbasbandy, S.; Shirzadi, A. (2011): MLPG method for two-dimensional diffusion equation with Neumann's and non-classical boundary conditions. *Appl. Numer. Math.*, vol. 61, pp. 170–180.

Atluri, S. N. (2004): *The Meshless Method, (MLPG) For Domain & BIE Discretizations*. Tech. Science Press, Forsyth.

Atluri, S. N.; Han, Z.; Shen, S. (2003): Meshless Local Patrov-Galerkin (MLPG) approaches for weaklysingular traction & displacement boundary integral equations. *CMES: Computer Modeling in Engineering & Sciences*, vol. 4, no. 5, pp. 507–517.

Atluri,S. N.; Shen, S. (2002): The Meshless Local Petrov-Galerkin (MLPG) Method: A Simple & Less-costly Alternative to the Finite Element and Boundary Element Methods. *CMES*, vol. 3, pp. 11–51.

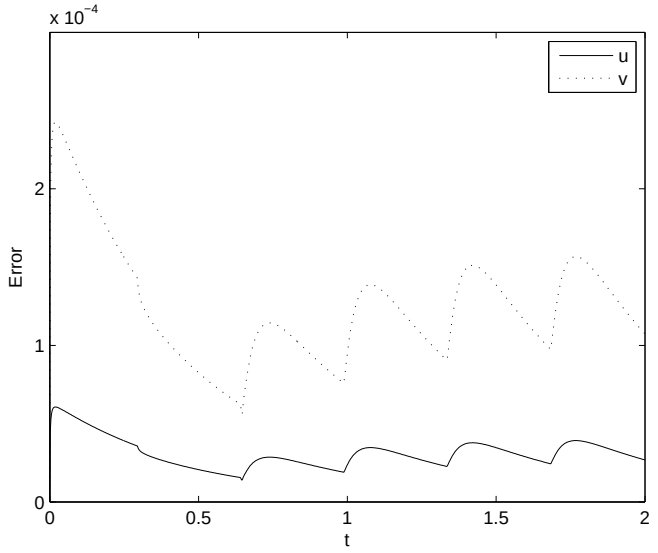

Figure 9: Max error of numerical solutions obtained by variable time steps with using the initial time step $\Delta t = 2^{-15}$ and the relaxation parameter $\tau = 0.002$

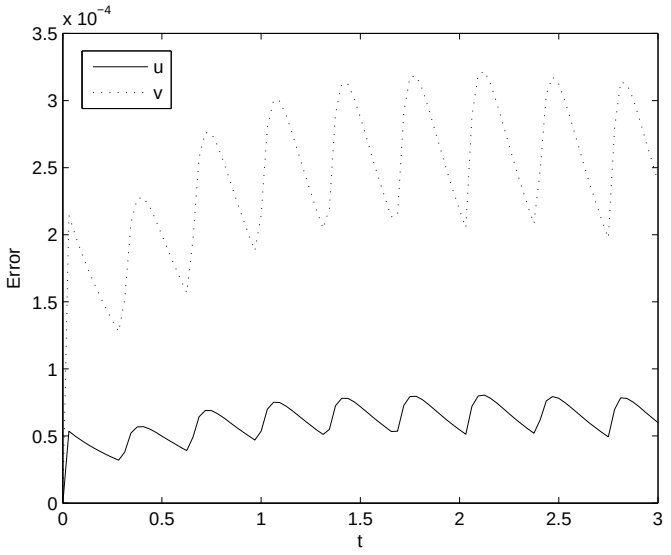

Figure 10: Max error of numerical solutions obtained by variable time steps with using the initial time step $\Delta t = 2^{-17}$ and the relaxation parameter $\tau = 0.004$

Brunner, H.; Ling, L.; Yamamoto, M. (2010): Numerical simulations of 2D fractional subdiffusion problems. *J. Comput. Phys.*, vol. 229, pp. 6613–6622.

Castets, V.; Dulos, E.; Boissonade, J.; De Kepper, P. (1990): Experimental evidence of a sustained Turing-type equilibrium chemical pattern. *Phys. Rev. Lett.*, vol. 64, pp 2953–2956.

Ching, H.-K.; Batra, R. C. (2001): Determination of crack tip fields in linear elastostatics by the meshless local Petrov-Galerkin (MLPG) method. *CMES: Computer Modeling in Engineering & Sciences*, vol. 2, pp. 273–289.

Ebeling, W. (1976): *Strukturbildung bei Irreversiblen Prozessen. Eine Einfürung in die Theorie dissipativer Strukturen.* BSB B.G. Teubner Verlagsgesellschaft, Leipzig.

Haken, H. (1975): Cooperative phenomena in systems far from thermal equilibrium and in nonphysical systems. *Rev. Mod. Phys.*, vol. 47, pp. 67–121.

Haken, H. (1978): *Synergetics - An Introduction, Nonequilibrium Phase Transitions and Self-Organization in Physics, Chemistry and Biology*. Springer-Verlag, Berlin.

Kondo, S.; Asai, R. (1995): A reaction-diffusion wave on the skin of the marine angelfish Pomacanthus. *Nature*, vol. 376, pp. 765–768.

Lancaster, P.; Salkauskas, K. (1981): Surfaces generated by moving least square methods. *Math. Comput.*, vol. 37, pp. 141–158.

Libre, N. A.; Emdadi, A.; Kansa, E. J.; Shekarchi, M.; Rahimian, M. (2009): A multiresolution prewavelet-based adaptive refinement scheme for RBF approximations of nearly singular problems. *Eng. Anal. Bound. Elem.*, vol. 33, pp. 901–914.

Ling, L.; Kansa, E. J. (2004): Preconditioning for radial basis functions with domain decomposition methods. *Math. Compt. Modelling*, vol. 40, no. 13, pp. 1413–1427.

Ling, L.; Hon, Y. C. (2005): Improved numerical solver for Kansa's method based on affine space decomposition. *Eng. Anal. Bound. Elem.*, vol. 29, no. 12, pp. 1077–1085.

Liu, G. R. (2003): *Mesh Free Methods, Moving Beyond the Finite Element Method*. CRC Press, Boca Raton.

Lotka, A. J. (1956): *Elements of Mathematical Biology*. Dover, New York.

Meinhardt, H. (2009): *The Algorithmic Beauty of Sea Shells*. 4th ed., Springer-Verlag, Berlin.

Miura, T.; Shiota, K.; Morriss-Kay, G.; Maini, P. (2006): Mixed mode pattern in Doublefoot mutant mouse limb-Turing reaction-diffusion model on a growing domain limb development. *J. Theor. Biol.*, vol. 240, pp. 562–573.

Moore, P. K.; Flaherty, J. E. (1992): Adaptive local overlapping grid methods for parabolic systems in two space dimensions. *J. Comput. Phys.*, vol. 98, no. 1, pp. 54–63.

Nicolis, G.; Prigogine, I. (1977): *Self-Organization in Nonequilibrium Systems*. John Wiley & Sons, New York.

Prigogine, I.; Nicolis, G. J. (1967): On symmetry-breaking instabilities in dissipative systems. *J. Chem. Phys.*, vol. 46, pp. 3542–3550.

Prigogine, I.; Lefever, R. (1968): Symmetry breaking instabilities in dissipative systems II. *J. Chem. Phys.*, vol. 48, pp. 1695–1700.

Ouyang, Q.; Swinney, H. (1991): Transition from a uniform state to hexagonal and striped Turing patterns. *Nature*. vol. 352, pp. 610–612.

Schlögl, F. (1971a): On stability of steady states. *Z. Physik*, vol. 243, pp. 303–310.

Schlögl, F. (1971b): On thermodynamics near a steady state. *Z. Physik*, vol. 248, pp. 446–458.

Schlögl, F. (1972): Chemical reaction models for non-equilibrium phase transitions. *Z. Physik*, vol. 253, pp. 147–161.

Segal, L.; Jackson, J. (1972): Dissipative structure: an explanation and an ecological example. *J. Theor. Biol.*, vol. 37, pp. 545–559.

Sladek, J.; Sladek, V.; Atluri, S. N. (2004): Meshless local Petrov-Galerkin method for heat conduction problem in an anisotropic medium. *CMES: Computer Modeling in Engineering & Sciences*, vol. 6, pp. 309–318.

Sladek, V.; Sladek, J.; Tanaka, M.; Zhang, C.-H. (2005): Transient heat conduction in anisotropic and functionally graded media by local integral equations. *Eng. Anal. Bound. Elem.*, vol. 29, pp. 1047–1065.

Sladek, J.; Sladek, V.; Tan, C. L.; Atluri, S. N. (2008): Analysis of transient heat conduction in 3D anisotropic functionally graded solids by the MLPG method. *CMES: Computer Modeling in Engineering & Sciences*, vol. 32, pp. 161–174.

Smith, G. D. (1978): *Numerical Solution of Partial Differential Equations: Finite Diffrence Methods*. Clarendon Press, Oxford.

Turing, A. M. (1952): The chemical basis of morphogenesis. *Phil. Trans. Roy. Soc.*, B237, pp. 37–72.

Volterra, V. (1931): *Lesons sur la theorie mathematique de la lutte pur la vie*. Gauthier-Villars, Paris.

Zhabotinskiy, A. M. (1964): Periodic processes of the oxydation of malonic acid in solution. *Biofizika*, vol. 9, pp. 306–311.

Zhu, T.; Zhang, J.-D.; Atluri,S. N. (1998): A local boundary integral equation (LBIE) method in computational mechanics, and a meshless discretization approach. *Computational Mechanics*, vol. 21, pp. 223–235.